

Single crystal growth of CeTAl_3 ($T = \text{Cu, Ag, Au, Pd and Pt}$)

C. Franz^{a,b,*}, A. Senyshyn^b, A. Regnat^a, C. Duvinage^a, R. Schönmann^a, A. Bauer^a, Y. Prots^c, L. Akselrud^c, V. Hlukhyy^d, V. Baran^d, C. Pfleiderer^a

^aPhysik Department, Technische Universität München, D-85747 Garching, Germany

^bHeinz Maier-Leibnitz Zentrum (MLZ), Technische Universität München, D-85748 Garching, Germany

^cMax-Planck Institut für die chemische Physik fester Stoffe (MPI CPFS), D-01187 Dresden, Germany

^dFakultät für Chemie, Technische Universität München, D-85747 Garching, Germany

Abstract

We report single crystal growth of the series of CeTAl_3 compounds with $T = \text{Cu, Ag, Au, Pd and Pt}$ by means of optical float zoning. High crystalline quality was confirmed in a thorough characterization process. With the exception of CeAgAl_3 , all compounds crystallize in the non-centrosymmetric tetragonal BaNiSn_3 structure (space group: $I4mm$, No. 107), whereas CeAgAl_3 adopts the related orthorhombic PbSbO_2Cl structure (Cmcm, No. 63). An attempt to grow CeNiAl_3 resulted in the composition CeNi_2Al_5 . Low temperature resistivity measurements down to ~ 0.1 K did not reveal evidence suggestive of magnetic order in CePtAl_3 and CePdAl_3 . In contrast, CeAuAl_3 , CeCuAl_3 and CeAgAl_3 display signatures of magnetic transitions at 1.3 K, 2.1 K and 3.2 K, respectively. This is consistent with previous reports of antiferromagnetic order in CeAuAl_3 , and CeCuAl_3 as well as ferromagnetism in CeAgAl_3 , respectively.

Keywords: Float zone technique, Single crystal growth, Rare earth compounds, Magnetic materials, Crystal structure determination, Electric resistivity

1. Introduction

Cerium-based intermetallic compounds represent an ideal testing ground for the study of novel electronic ground states and unusual low-lying excitations, where valence fluctuations, heavy-fermion behaviour, unconventional superconductivity and exotic forms of spin and charge order are ubiquitous. Despite many decades of intense research, the understanding of the nature of strong electronic correlations in Ce-based systems, at best, may be referred to as being qualitative. A scenario that is widely alluded to when addressing correlations in f-electron systems considers the competition of Ruderman-Kittel-Kasuya-Yosida (RKKY) interactions, supporting magnetic order, with the single-impurity Kondo effect quenching magnetic moments. While there have been various attempts to advance the understanding, simultaneous treatment of multiple, nearly equivalent energy scales

such as exchange and dipolar interaction, spin-orbit coupling, crystal electric fields and strong magneto-elastic coupling has not been attempted.

Given this general context, the class of CeTX_3 , where T is a transition metal element and X a simple metal, offer important new insights. For instance, selected members of this series have been discovered, which exhibit a coexistence of magnetic order and superconductivity under pressure. Another line of research pursues the strong coupling of phonons with relatively low lying crystal electric fields (CEF) levels. An important example has been reported in CeCuAl_3 [2], which was interpreted in terms of a quasi-bound vibron state first observed in CeAl_2 [24, 38]. However, recent studies in CePd_2Al_2 , as well as preliminary work in other members of the CeTX_3 series suggest, that strong interactions of the crystal fields with the spectrum of phonons somewhat akin the claim of vibrons in CeCuAl_3 is more generic than assumed so far.

In this paper we report single crystal growth of the series CeTAl_3 with $T = \text{Cu, Ag, Au, Pd and Pt}$.

*Corresponding author. +49 89 289 14760

Email address: christian.franz@frm2.tum.de (C. Franz)

For our study we have used optical float zoning, to the best of our knowledge, for the first time. Following a thorough characterisation, we determine the crystal structure of the systems studied. The high sample quality achieved in our study is corroborated in measurements of the electrical resistivity, which was performed at temperatures down to 0.1 K.

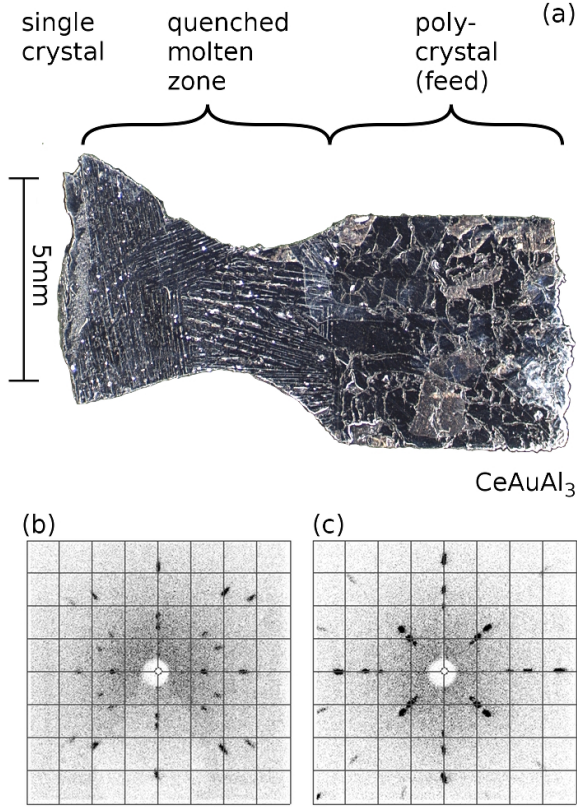


Figure 1: (a) Cut through the quenched final zone of the CeAuAl₃ crystal along the rotational symmetry axis. Polycrystalline part of the feed rod, quenched molten zone and beginning of the single crystal are visible. The quenched molten zone features a pronounced stripe pattern. Laue X-ray images along crystallographic a- and c-axes are shown in panels (b) and (c), respectively.

All crystal structures reported in literature for the series of CeTAl₃ compounds are derived from the BaAl₄ structure, depicted in fig. 2(a). The BaAl₄ structure crystallizes tetragonal body-centred with eight Ce-atoms at the corners and one in the center. The aluminum atoms are arranged in six planes parallel to *ab* in the unit cell. The following three important types of structures may be derived from the BaAl₄ structure in which the

Al and T atoms are ordered.

(i) The ThCr₂Si₂ (*I*₄/*mmm*) structure, shown in Fig. 2(b) is currently most frequently reported for intermetallic compounds. The sequence of layers along the *c*-direction is given as A - [X-T-X] - A with A a rare-earth metal, T the transition metal element and X either Si, Ge or Al. Typical examples include CeT₂X₂ compounds (CeCu₂Si₂ [13], CeCu₂Ge₂ [12], CePd₂Si₂, CeRh₂Si₂ [6]) as well as URu₂Si₂ [9] and BaFe₂As₂ [33].

(ii) The CaBe₂Ge₂ (*P*₄/*nmm*) variant of the BaAl₄ structure, shown in Fig. 2(c)), is also characterised by full inversion symmetry and a layered structure along the *c*-axis following the sequence A - [X-T-X] - A - [T-X-T] - A. The CaBe₂Ge₂ structure is less frequently found because different atom sizes can not be matched very well in contrast to ThCr₂Si₂ [15]. An important example of immediate relevance to the Al-based compounds addressed in our study is CePd₂Al₂ [22].

(iii) The BaNiSn₃ (*I*₄*mm*) structure is the only subtype with lacking inversion center. In recent years Ce-systems with a BaNiSn₃-type structure have generated great interest, since the discovery of superconductivity in heavy fermion systems such as CeIrSi₃, CeRhSi₃ [40], CeCoGe₃ [10]. In these systems the superconducting pairing symmetry may be outside traditional classification schemes. Shown in Fig. 2(d) is the characteristic unit cell, where the stacking sequence of layers is A-T-X(1)-X(2)-A-T-X(1)-X(2)-A may be readily seen. The point group of these systems is C_{4v}, lacking a mirror plane.

In the following, a brief overview over the literature on CeTAl₃ compounds is given. Key properties reported are summarised in table 1. The crystal structure has been determined as *I*₄*mm* in CeAuAl₃ as well as CeCuAl₃ in both poly- and single crystals. For CeAgAl₃ no distinction has been possible between *I*₄*mm* and *I*₄/*mmm*, whereas CePtAl₃ was reported to adopt a centrosymmetric variant *I*₄/*mmm*. Interestingly, CePdAl₃ was reported to crystallize in the orthorhombic *Fmm*2 structure.

Compared to the textbook examples of 3d magnets, crystal electric fields in 4f compounds are weak. Nevertheless, the crystal fields influence the magnetic properties of 4f systems rather strongly. By Hund's rule, Ce³⁺ has a six-fold degenerate ground state, split into three Kramers doublets by the tetragonal crystal field. In CeCuAl₃ it has been reported that they are low lying with Δ₁=15 K and Δ₂=238 K [8, 25]. Further for CeAuAl₃ excited levels of Δ₁=57 K and Δ₂=265 K [32] as well as

	Mag	crystal	space group	$T_{C/N}$ (K)	T_K (K)	γ (mJ/molK ²)	μ_{eff} (μ_B)	μ_{CW} (μ_B)
CeCuAl ₃	AFM	pc, sc	$I4mm$ [27, 26, 21]	2.1 [8, 23]	8 [8]	140 [8]	1.8 [26]	2.61 [8]
CeAuAl ₃	AFM	pc	$I4mm$ [17, 32, 37]	1.32 [32]	4.5 [32]	227 [32]	2.1 [26]	2.6 - 2.8 [37]
CeAgAl ₃	FM	pc	$I4/mmm$ or $I4mm$ [28]	3.2 [28]	-	-	-	2.23 [28]
CePdAl ₃	AFM	pc	$Fmm2$ [34]	6 [34]	-	-	-	-
CePtAl ₃	SG	pc	$I4/mmm$ [26, 16]	0.8 [16, 34]	-	-	1.8 [26]	2.08 [16]

Table 1: Resume of CeTAl₃ properties in literature. AFM - antiferromagnetism, FM - ferromagnetism, SG - Spin-Glass; pc - polycrystal, sc - singlecrystal; $T_{C/N}$ - Curie/Neel-temperature, T_K - Kondo-temperature; μ_{eff} - effective moment, μ_{CW} - Curie-Weiss moment

$\Delta_1 = 60$ K and $\Delta_2 = 240$ K [37] have been reported.

Magnetic ground states in CeTX₃ compounds are usually antiferromagnetic, as in CeCuAl₃ with $T_N = 2.1$ K and CeAuAl₃ with $T_N = 1.32$ K. However, the exact magnetic ground states are more complicated, with a propagation vector $\mathbf{k} = (0.4, 0.6, 0)$ in the case of CeCuAl₃ [20] and $\mathbf{k} = (0, 0, 0.52)$ for CeAuAl₃ [1]. CeAgAl₃ is a rare example of ferromagnetic Ce-compound below the ordering temperature of $T = 3.2$ K. CePdAl₃ is reported to order antiferromagnetically below 6 K, CePtAl₃ exhibits spin-glass behaviour below 0.8 K.

All magnetic compounds possess an easy *ab*-plane and hard *c*-axes. Kondo temperatures have been determined in CeCuAl₃ at 8 K and CeAuAl₃ at 4.5 K, where a weak screening of less than 25 % has been found in an ²⁷Al-NMR study [39]. Both compounds show a heavy fermion ground state, demonstrated by an electronic contribution to the specific heat of $\gamma = 227$ mJ/molK² as well as a large prefactor of the low-temperature electric resistivity of $A = 5.0 \mu\Omega\text{cm/K}^2$ in CeAuAl₃ [32] and $\gamma = 140$ mJ/molK² in CeCuAl₃. Under pressure, T_N rises up to 60 kbar in CeCuAl₃ and suddenly vanishes at 80 kbar [18, 30], pointing towards the existence of a quantum critical point (QCP). Recently, a phonon - crystal field quasibound state has been found in CeCuAl₃ [2], which is not present in CeAuAl₃ [1]. Furthermore, a low energy anomalous excitation [4] and phonon scattering by Ce magnetic moment fluctuations are reported in CeAuAl₃ [5], as well as a possible second phase transition at 0.18 K [1].

2. Experimental Methods

The physical properties of rare earth containing compounds tend to be very sensitive to defects and impurities. In turn, we have made great efforts to reduce such defects and impurities to the lowest possible level. Notably, the procedure of the single-crystal preparation is based on the use of high purity starting elements and a bespoke workflow that is optimised to minimise contamination by oxygen. As the perhaps most important aspect, we have used optical float-zoning (OFZ) representing a crucible-free technique.

Metal lumps of Ce (Ames, 99.9995%), shots of Au and Ag (AlfaAesar Premion, 99.995% 99.9999%), lumps of copper (MaTecK, 99.9999%), powder of Pd and Pt (AlfaAesar Premion, both 99.995%) and lumps of Al (MaTecK, 99.9999%) were used for the preparation of the feed and seed rods. Ce and Al were weighted in an argon glove box system. First CeAl₂ was prepared in an induction heated horizontal copper cold boat system that can be loaded by means of a bespoke load-lock from a glove box [7]. This reduces contamination of the Ce with oxygen, as the educt CeAl₂ is stable on air. In a second step, the CeAl₂ was then reacted with the transition metals $T = \text{Au, Ag, Cu, Pt or Pd}$ and additional Al in a water cooled Hukin-type radio frequency heated copper crucible.

The sample was remelted and flipped over several times to assure a good homogeneity. The resulting pill was subsequently cast into cylindrical feed and seed rods with a diameter of 6 mm and a length of 40 to 60 mm's. Furthermore, synthesis of a polycrystalline sample of CeNiAl₃ was attempted by means of our rod casting furnace. For CeAuAl₃ the ternary compound was prepared with-

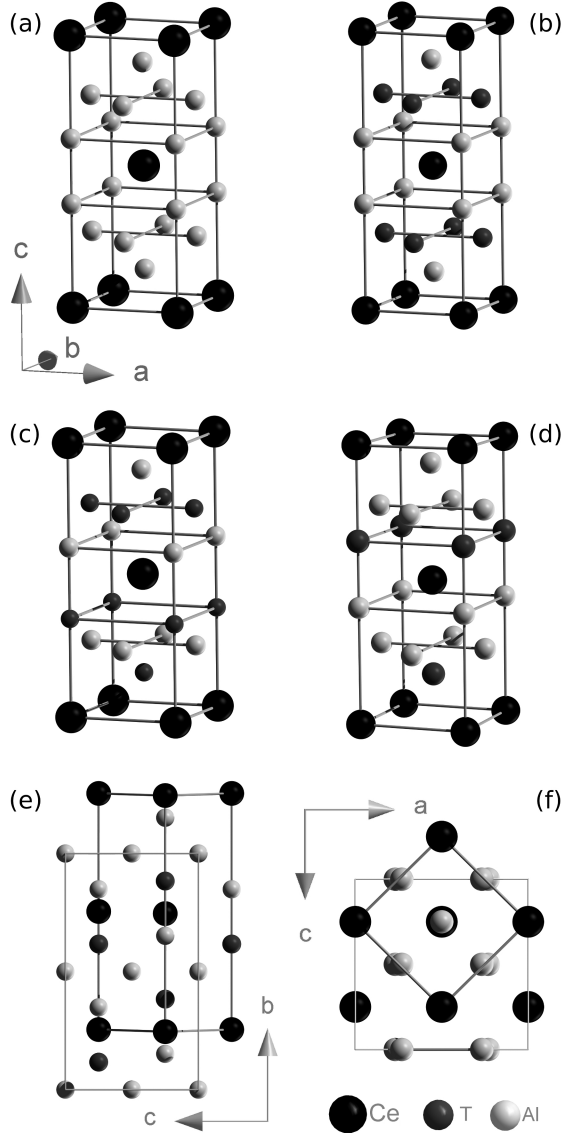


Figure 2: Overview over the BaAl_4 parent structure and important subtypes derived of this structure. (a) BaAl_4 with space group $I4/mmm$ and full inversion symmetry. (b) ThCr_2Si_2 with space group $I4/mmm$ and full inversion symmetry. (c) CaBe_2Ge_2 with space group $P4/nmm$ and full inversion symmetry. (d) BaNiSn_3 with space group $I4mm$, lacking inversion symmetry. (e) and (f) Schematic representation of the BaNiSn_3 structure type and the Cmcm (PbSbO_2Cl) structure type.

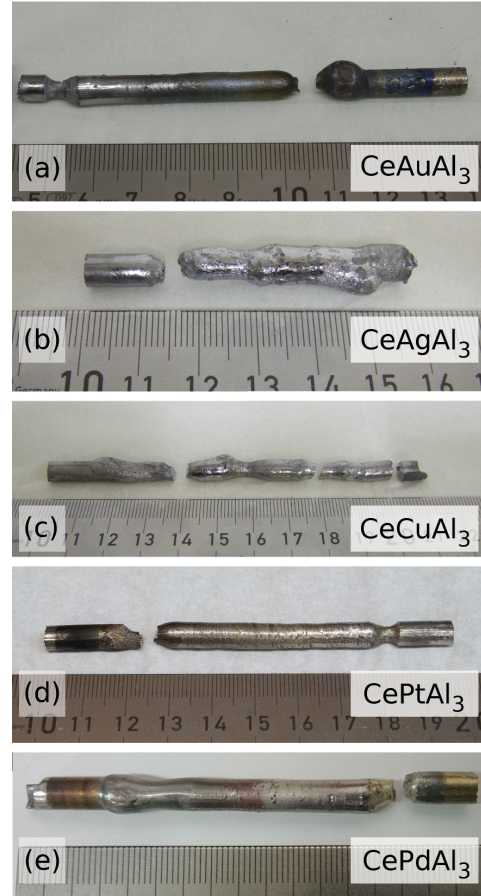


Figure 3: Photographs of all crystals grown by optical float zoning for this study. Scale in cm. (a) CeAuAl_3 (b) CeAgAl_3 (c) CeCuAl_3 (d) CePtAl_3 (e) CePdAl_3

out the intermediate step of first synthesising CeAl_2 by means of the glove box and the horizontal cold boat system and the bespoke load-lock.

The actual single crystal growth was performed in a CSI 4-mirror (model FZ-T 10000-H-III-VPS) optical float zone furnace. The furnace was re-designed to be all-metal sealed. Prior to growth the furnace was baked with bespoke heating jackets [29]. 500 W halogen lamps were used for the growth process under a static argon atmosphere at a pressure of 2.5 bar. The float zoning was performed with a growth rate of 5 mm/h and a counter rotation of 6 rpm of the feed and seed rod, respectively.

The characterization of the crystals proceeded as follows. First, all crystals were examined under an optical light microscope. Laue X-ray (Multi-wire Laboratories MWL 110) images were taken on different spots covering all of the surface of the in-

got to identify the single crystalline part and possible grain boundaries. In CeAuAl_3 additionally cross sections of the upper and lower part of the crystal were analysed as well as a cut through the quenched final part of the molten zone. Figure 1 (a) shows from right to left the polycrystalline feed rod, the quenched molten zone with a pronounced stripe structure and the beginning of the single crystal at the lower end.

All crystals were oriented by Laue X-ray diffraction. Fig. 1(b) and (c) show typical Laue pictures of CeAuAl_3 for the a - and c -axes, respectively. The composition was confirmed by single crystal and powder x-ray diffraction. For CeAuAl_3 additional scanning electron microscope images and energy dispersive X-ray spectra were recorded.

Small single crystals with dimensions less than $100\text{ }\mu\text{m}$ were mechanically extracted from CeTAl_3 ($T = \text{Cu, Ag, Au, Pd}$ and Pt) ingots as grown. Generally all tested crystals were of high quality with sharp diffraction peaks. Intensity data were collected with graphite-monochromatized $\text{Mo K}\alpha$ X-ray radiation. Three-dimensional data were indexed, integrated and corrected for Lorentz-, polarization, absorption and background effects using a diffractometer specific software, namely CrystalClear for a Rigaku Saturn724+ and X-Area for a STOE IPDS II. Initial structure analysis/solution (using direct methods) for CeTAl_3 ($T = \text{Ag, Au, Cu, Pt}$) was done with SHELX-2012 as implemented in the program suite WinGX 2014.1 [14]. The crystal structure of modulated CePdAl_3 was solved using WinCSD [3]. The experimental data and results of the structure refinement for selected samples are reported in table 3, while the fractional atomic coordinates, occupation numbers and equivalent isotropic, and anisotropic atomic displacement parameters are listed in table 4 and 5.

Samples for resistivity measurements were cut from the single-crystalline sections of the ingots with a diamond wire saw. Typical dimension of the samples were 4 to 6 times 1 times 0.2 mm^3 , oriented such that the electrical current could be applied along longest direction which corresponding to the c -axis. The resistivity was measured in a standard four-probe ac-configuration using a digital lock-in amplifier and an excitation current of 5 mA at an excitation frequency of 22.08 Hz. Room temperature transformers were used for impedance matching. Data were recorded between 2 K and 300 K in a standard ^4He cryostat. Data down to much lower temperatures were measured for

CeTAl_3 with $T = \text{Cu, Ag, Au}$ in an adiabatic demagnetisation refrigerator (ADR) using the same detection technique at a lower excitation current of 1 mA down to a temperature below $\sim 300\text{ mK}$. For samples with $T = \text{Pt, Pd}$ a $^3\text{He}/^4\text{He}$ dilution refrigerator was used down to temperatures well below 100 mK.

3. Experimental Results

3.1. Crystal Structure

The actual growth process resulted in the ingots shown in Fig. 3. We obtained large single crystals of CeAuAl_3 , CeCuAl_3 and CePtAl_3 shown in Figs. 3 (a), (c) and (d), respectively. While these ingots remained mechanically intact after growth, the CeCuAl_3 ingot (shown in Fig. 3 (a)) broke spontaneously in one location during cool-down after growth. For CeAgAl_3 single crystalline grains were prepared from the ingot. The melt in the growth process of CePdAl_3 was very unstable and we could only prepare small single crystalline samples with a typical size of up to 3 mm. A second attempt to grow CePdAl_3 with a reduced growth rate of 1 mm/h allowed to obtain the large single crystal depicted in Fig. 3 (e). Note that all measurements on CePdAl_3 reported in this paper were carried out on samples cut from the first crystal.

The analysis of the arrays of the diffraction data revealed that the majority of the CeTAl_3 compounds ($T = \text{Au, Cu, Pt}$) studied display reflections consistent with the tetragonal lattice and in line with one of distorted BaAl_4 structure types. The T/Al antisite disorder essentially corresponds to the local differences between ThCr_2Si_2 , CaBe_2Ge_2 , HoCuAl_3 or BaNiSn_3 structures. Extinction of characteristic reflections revealed a body centred tetragonal lattice and the structure solution corresponded to a BaNiSn_3 type structure for CeAuAl_3 , CeCuAl_3 and CePtAl_3 . Evidence for putative Au/Al antisite disorder in CeAuAl_3 was below the detection limit, whereas for CeCuAl_3 a small Cu/Al mixing on the copper site was observed consistent with a $\sim 5\%$ site occupation factor (sof) deficiency on the 4b Al site. A higher degree of antisite disorder was found in our CePtAl_3 sample. Assuming a stoichiometric composition and fully occupied atomic sites of CePtAl_3 , the antisite Pt/Al disorder appears to be as high as 18 % sof at both T and Al 2a sites. The obtained unit cell volumes were found to decrease in the series $\text{Au} - \text{Pt} - \text{Cu}$ in accordance

with the metallic radii ($r_{Au} = 1.44 \text{ \AA}$, $r_{Pt} = 1.39 \text{ \AA}$, $r_{Cu} = 1.28 \text{ \AA}$).

For $CeAgAl_3$ a small orthorhombic distortion of the $BaAl_4$ type lattice was detected of order $\sim 0.1 \text{ \AA}$. The character of the reflection splitting and the extinction revealed a C-base centred orthorhombic lattice with $a_0 \approx a_T\sqrt{2}$, $b_0 \approx c_T$ and $c_0 \approx a_T\sqrt{2}$, where O and T correspond to orthorhombic and tetragonal lattice dimensions. The structure solution corresponds to the $Cmcm$ space group and a model consistent with the structure type of $PbSbO_2Cl$. The orthorhombic superstructure observed occurs in oxyhalides and is found rarely in intermetallics, e.g., in $LaZn_4$ [31] and $SrPdGa_3$ [35]. Similar to $CeCuAl_3$ a small Ag/Al mixing occurs on the Ag site along with a weak (ca. 4% sof) deficiency on the 8e Al site.

A comparison of the Ag and Au based $CeTAl_3$ structures is plotted in Fig.2(e) and (f). We note, that Ag and Au nominally possess the same metallic radii ($r_{Ag} = 1.44 \text{ \AA}$), which may correspond to a similar magnitude of chemical pressure in both $CeTAl_3$ ($T = Au, Ag$). Indeed, the normalised lattice dimensions of $CeAgAl_3$ ($a_T \approx (a_0 + b_0)/2\sqrt{2} \approx 4.3566(8) \text{ \AA}$, $c_T \approx 10.837(2) \text{ \AA}$) are very similar to those of $CeAuAl_3$. Further, the relative cerium and aluminium positions reproduce well, whereas major differences were noticed for the distribution of gold and silver sites. By their arrangement the structure may be viewed as an intermediate step between $BaAl_4$ (or $HoCuAl_3$) and the $BaNiSn_3$ structure type. The antisite disorder observed smears out the layered structure along the c -axis in $CeAgAl_3$, which initially can be described as A - [TX-X-TX] - A, where TX indicated mixed T and X layer occupation.

The set of Bragg reflections collected for our single crystal of $CePdAl_3$ could neither be described with a conventional tetragonal nor with orthorhombic lattices. Careful indexing reveals a tetragonal cell with a c -parameter comparable to $CeTAl_3$ ($T = Au, Ag, Cu, Pt$), however, with an a lattice parameter multiplied by a factor of ~ 3 . Analysis of peak systematics resulted in a solution corresponding to a body centred tetragonal lattice. This is in agreement with group theory, as the $3a$, c axis multiplication in the $I4mm$ space group is allowed in the frame of klassengleiche subgroups IIc for $I4mm$ ($3a$ structure). Multiplication of the axis results in a splitting of the Ce and Pd positions into three independent sites, whilst the two initial aluminium

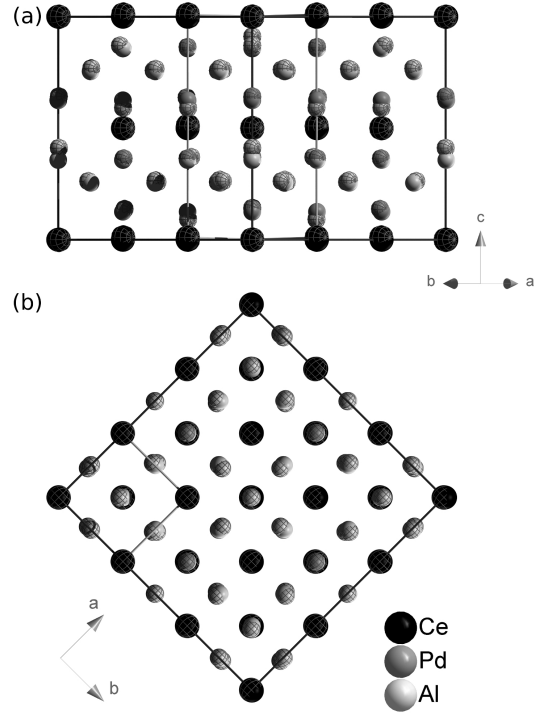


Figure 4: Refined structural modifications of $CePdAl_3$: plane atoms - $BaNiSn_3$ type of structure, structured atoms - klassengleiche subgroup of $BaNiSn_3$ type of structure with $3a$ multiplied axis.

sites are split into seven positions in the larger cell. Similar to $CeCuAl_3$, $CePtAl_3$, $CeAgAl_3$ Rietveld refinement corresponded to a Pd/Al antisite disorder, where, however, only one Pd site of three as well as two of the seven Al sites were affected.

Examination of a crushed and pulverized ingot using lab X-ray powder diffraction did not reveal any hints for a $3a$ structure, but a conventional $BaNiSn_3$ modification for $CePdAl_3$ (see Table 5). The crystal structures of both the $BaNiSn_3$ -type and the $3a$, c axis multiplied modifications of the $CePdAl_3$ structures are shown in Fig.4. The $Ce(0,0,0)$ atomic position is here used as a reference. In comparison to the $BaNiSn_3$ -type modification of $CePdAl_3$, the $3a$ structure contains a certain degree of Pd/Al disorder and by its layer structure A - [TX-X-TX] - A it becomes very similar to $CeAgAl_3$. An attempt to refine the structure modulation in $CePdAl_3$ was performed assuming both commensurate and incommensurate modulation vectors of the $BaNiSn_3$ parent structure. The

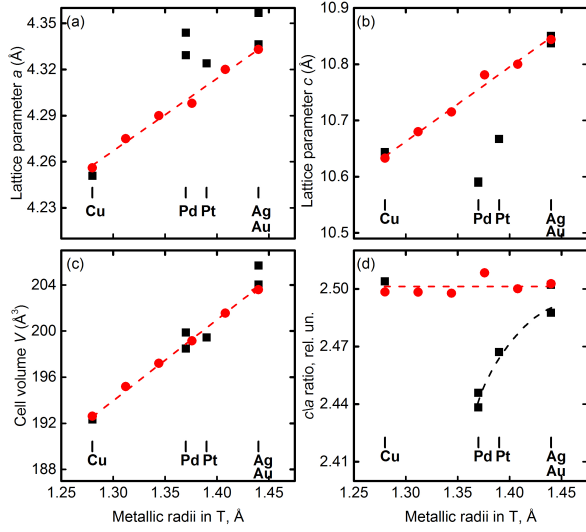


Figure 5: Lattice parameter, cell volume and c/a ratio for different CeTAl_3 ($T = \text{Ag, Au, Cu, Pd, Pt}$) plotted as a function of T metallic radius (black squares). Data showed by red circles correspond to $\text{CeAu}_{1-x}\text{Cu}_x\text{Al}_3$ solid solution taken from [19]. Two data points for CePdAl_3 correspond to BaNiSn_3 and 3a structures. The lines are showed as guides for the eyes.

atomic modulated displacements were comparable to standard uncertainties of atom localization and improvement to fit residuals (when compared to the structure model with $3a$, c axis multiplication), and thus, found to be marginal.

The lattice parameters of the CeTAl_3 ($T = \text{Ag, Au, Cu, Pd, Pt}$) samples studied were found to be in a good agreement with experimental data reported in Refs. [19, 27, 41, 25, 23]. Cell volumes in CeTAl_3 ($T = \text{Ag, Au, Cu, Pd, Pt}$) follow a linear dependence as a function of T ionic radii (see Fig. 5) in line with values reported for the CeAuAl_3 to CeCuAl_3 pseudobinary system [19], which displays a behaviour characteristic of Vegard's law. The observed linear dependence may be viewed in terms of structural changes in CeTAl_3 ($T = \text{Ag, Au, Cu, Pd, Pt}$) driven by chemical pressure. However, all CeTAl_3 studied are characterised by a large anisotropy. Notably, for CeCuAl_3 , CeAuAl_3 and corresponding solid solutions [19] the c/a ratio is nearly constant with $c/a \sim 2.5$. This compares with CePdAl_3 , CePtAl_3 and CeAgAl_3 , which display lower c/a values.

Taking a separate look on the experimentally determined lattice parameters indicates a parameters that are systematically reduced, as well as c

	ρ_0 ($\mu\Omega\text{cm}$)	RRR	$\rho_{300\text{ K}}$ ($\mu\Omega\text{cm}$)
CeAuAl_3	15.18	2.50	37.8
CeCuAl_3	12.9	2.84	36.6
CeAgAl_3	7.9	3.81	30.1
CePdAl_3	25.1	1.39	35.0
CePtAl_3	67.4	1.25	84.1

Table 2: Parameters derived from resistivity measurements on CeTAl_3 with $T = \text{Au, Cu, Ag, Pd}$ and Pt . ρ_0 is the residual resistivity extrapolated to $T = 0$, RRR the residual resistivity ratio $\rho(300\text{ K})/\rho_0$, where $\rho(300\text{ K})$ denotes the resistivity at room temperature.

lattice parameters that are systematically smaller than those observed in the $\text{CeAuAl}_3 - \text{CeCuAl}_3$ pseudobinary system. Taking into account nominally equal metallic radii for Au and Ag , the differences observed for the a lattice dimensions and cell volume of CeAuAl_3 and CeAgAl_3 as well as their different structure, significantly reduces the relevance of an approximation in the spirit in terms of chemical pressure and shows that the chemical nature of T in CeTAl_3 plays a dominant role for the structure and its distortion.

3.2. Electric Resistivity

Shown in Fig. 6 (a1) to (a5) is the electric resistivity for CeTAl_3 with $T = \text{Cu, Ag, Au, Pd}$ and Pt covering three decades of temperature from $\sim 0.1\text{ K}$ to 300 K . For these data the electrical currents were applied parallel to the crystallographic c -axis. Further, Fig. 6 (b1) - (b5) shows the same data on a temperature scale up to 20 K for a better visibility of the low temperature features.

All samples show metallic behaviour over the complete temperature range. The residual resistivity, resistivity at 300 K and associated residual resistivity ratios (RRR) of all compounds are summarized in table 2. The residual resistivity ratios below 5 for all compounds and are in good agreement with the literature. Observed values have been found lower than in Si or Ge based compounds, probably due to the remaining antisite disorder in our samples. We wish to note that preliminary work suggests, that careful annealing studies and tiny compositional adjustments to the starting compositions as well as variations of the parameters used for single crystal growth promise considerable improvements to these values.

The key features observed in the temperature dependences may be summarised as follows. For CeAuAl_3 the resistivity decreases of from 300 K to

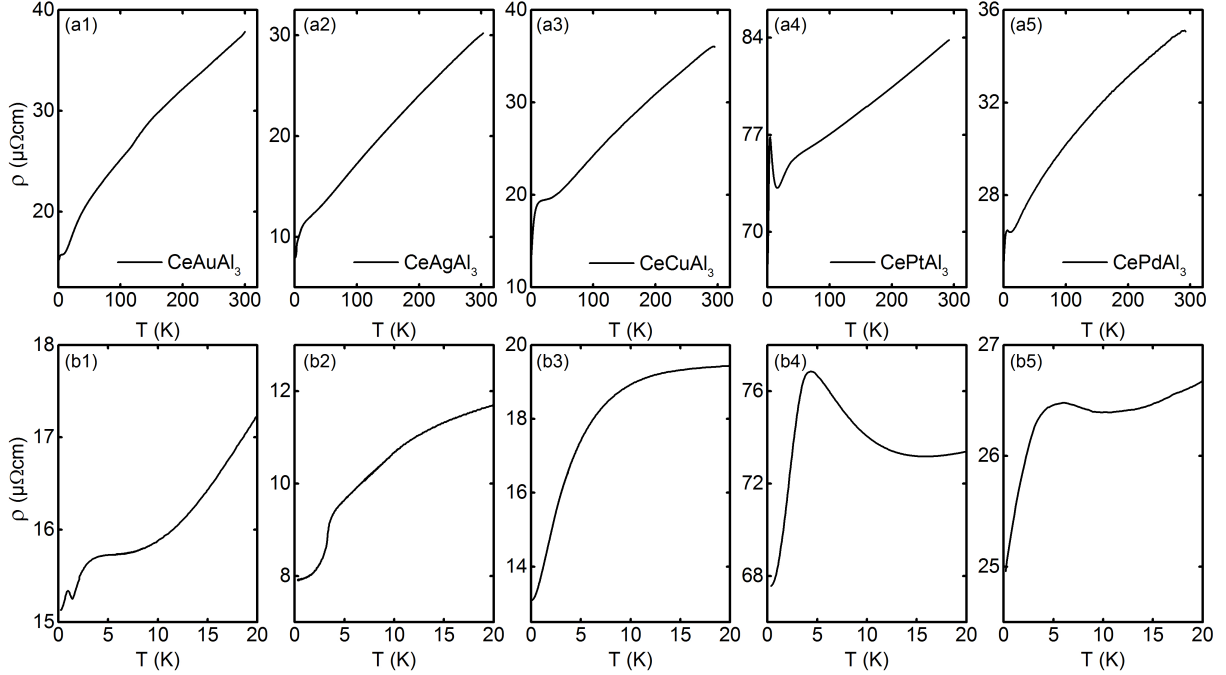


Figure 6: Electric resistivity for CeTAl_3 with $T = \text{Cu, Au, Ag, Pd, Pt}$. (a1) - (a5) On a large temperature range from $T_{\min} = 300 \text{ mK}$ to 300 K all samples show metallic behaviour. (b1) - (b5). Close-up view of the behaviour at low temperatures up to 20 K .

15 K in a quasi-linear manner, probably due to crystal electric field levels as discussed in ref. [32]. With decreasing temperature the decrease of the resistivity is followed by a plateau around 8 K and another strong decrease below the onset of magnetic order at 1.32 K . However the onset of the decrease at 4.5 K is considerably higher than T_c and maybe attributed to the coherence of a Kondo lattice. At $\sim 1 \text{ K}$, an additional maximum due to the opening of a super-zone gap is observed reminiscent of behaviour observed in CeGe [11] and Cr [36].

A linear decrease is observed in CeAgAl_3 down to approximately 17 K , followed by a steeper linear decrease. The change of slope is of unknown origin, but may be due to the changes of the coupling with the lattice degrees of freedom. A clear kink at 3.2 K , corresponding to the magnetic transition temperature of ferromagnetic order reported in the literature, is followed by a quadratic temperature dependence down to lowest temperatures. The specific temperature dependence may be characteristic of weakly spin-polarised Fermi liquid, where electron magnon scattering is weak.

In CeCuAl_3 the linear decrease at high tem-

peratures is followed by a plateau between 30 K and 10 K , whereas a clear maximum as reported in Refs [23, 20] is not observed. The strong decrease below 10 K traditionally would be attributed to the coherence of a Kondo lattice, where a clear signature of the magnetic ordering transition at 2.1 K is not observed and maybe hidden by this Kondo coherence. However, on a speculative note an alternative scenario may be related to the strong electron-phonon interactions associated with the quasi-bound vibron. Below 0.5 K the decrease flattens towards a residual resistivity of $12.9 \mu\Omega\text{cm}$, which is among the lowest reported in the literature for this compound.

The linear decrease of the resistivity in CePtAl_3 down to $\sim 50 \text{ K}$ is followed by a stronger decrease to a minimum at 15.9 K . The origin of this kink may again be referred to as a Kondo coherence effect and yet, as speculated above, related to changes of the coupling to the crystal lattice. A logarithmic increase to a maximum at 4.3 K is most probably due the onset of Kondo scattering and followed by a strong decrease suggesting again Kondo coherence. Towards lowest temperatures, the decrease

flattens and is extrapolated to a residual resistivity of $25.1 \mu\Omega\text{cm}$. Overall, the resistivity is about a factor of three higher than for other compounds studied, which may be due to the higher degree of antisite disorder. There are no signs suggesting magnetic order, however below ~ 0.8 K the decrease of the resistivity flattens out.

Last but not least, CePdAl_3 shows a sublinear decrease over the entire temperature range, probably due to crystal field effects. The overall behaviour with a faint maximum around 5.7 K and strong decrease down to the lowest temperatures very much resembles the behaviour of CePtAl_3 . However, both the maximum and the decrease to lowest temperatures are less pronounced. Towards the lowest temperatures there is a linear decrease of the resistivity instead of a flattening out. As for CePtAl_3 we do not observe any features suggesting magnetic order.

4. Conclusions

Single crystals of the non-centrosymmetric intermetallic compounds CeTAl_3 ($T = \text{Cu, Ag, Au, Pd}$ and Pt) were grown. All samples were grown by means of optical float-zoning, to the best of our knowledge for the first time. Large single crystals were obtained for all compounds except CeAgAl_3 . For CePdAl_3 the growth rate had to be reduced from 5 mm/h to 1 mm/h to be stable. An attempt to grow a poly-crystal of CeNiAl_3 resulted in the compound CeNi_2Al_5 . The crystal structure was determined by single crystal and powder X-ray diffraction. The crystal structure is $I4mm$ in all cases except for CeAgAl_3 , which shows a small distortion corresponding to the orthorhombic $Cmcm$ structure. Further, the space group of CePdAl_3 has a three fold multiplied lattice parameter a , which is allowed by group theory. Although the unit cell volume follows the metallic radii of the transition metal element rather well, the c/a ratio is deviating strongly.

Site-antisite disorder of the T and X-site appears to be nominally absent in CeAuAl_3 , but reaches a value as high as 18% in CePtAl_3 , accounting for the larger residual resistivities as compared to the Si and Ge based compounds in this series. While the sample quality of our samples as grown is already high, we expect that careful studies addressing the precise growth conditions and role of post-growth treatment, such as annealing and/or electro-transport, promise significant improvements.

Further, resistivity measurements as described in the traditional language used for Ce-based compounds are consistent with Kondo behaviour for all samples except CeAgAl_3 . The occurrence of the Kondo maximum depends thereby on the transition metal element and is most pronounced for $T = \text{Pt}$. It is interesting to speculate, if, what seems to be Kondo-like behaviour, eventually turns out to be due to strong electron-phonon coupling as related to the notion of the quasi-bound vibron state reported in CeCuAl_3 . As a final point, features in the resistivity of CeAuAl_3 , CeCuAl_3 and CeAgAl_3 at low temperatures are consistent with published reports of antiferromagnetic order in the former two compounds and ferromagnetism in the latter system, respectively. This contrasts the literature on CePtAl_3 and CePdAl_3 , where we do not find signs of magnetic order down to 0.1 K in the resistivity, whereas spin glass order has been reported for CePtAl_3 and antiferromagnetic order for CePdAl_3 .

Taken together all single-crystals are of high quality consistent with very low residual resistivities as compared to the literature. This demonstrates that optical float-zoning as employed under pure conditions provides an excellent method for the preparation of Ce-based intermetallic compounds.

5. Acknowledgements

We wish to thank Matthias Ruderer for access to the glove box of E13, Rainer Jungwirth (FRMII) for EDX measurements on CeAuAl_3 , the TUM crystal lab for crystal orientation with Laue X-ray and preparation of the samples. Financial support of the Deutsche Forschungsgemeinschaft and DFG TRR80 are gratefully acknowledged.

References

References

- [1] D. T. Adroja, C. de la Fuente, A. Fraile, A. D. Hillier, A. Daoud-Aladine, W. Kockelmann, J. W. Taylor, M. M. Koza, E. Burzurí, F. Luis, J. I. Arnaud, and A. del Moral. Muon spin rotation and neutron scattering study of the noncentrosymmetric tetragonal compound CeAuAl_3 . *Phys. Rev. B*, 91:134425, Apr 2015.
- [2] D. T. Adroja, A. del Moral, C. de la Fuente, A. Fraile, E. A. Goremychkin, J. W. Taylor, A. D. Hillier, and F. Fernandez-Alonso. Vibron Quasibound State in the Noncentrosymmetric Tetragonal Heavy-Fermion Compound CeCuAl_3 . *Phys. Rev. Lett.*, 108:216402, May 2012.

- [3] Lev Akselrud and Yuri Grin. WinCSD: software package for crystallographic calculations (Version 4). *Journal of Applied Crystallography*, 47:803–805, 2014.
- [4] Y. Aoki, M. A. Chernikov, H. R. Ott, H. Sugawara, and H. Sato. Thermal conductivity of CeAuAl₃: Evidence of phonon scattering by Ce magnetic moment fluctuations. *Phys. Rev. B*, 62:87–90, Jul 2000.
- [5] Y. Aoki, S.R. Saha, T.D. Matsuda, H. Sugawara, and H. Sato. Anomalous low-energy excitation in CeAuAl₃. *Physica B: Condensed Matter*, 281-282(0):110 – 111, 2000.
- [6] Astier G. Ballestracci R. Etude cristallographique des siliciures ternaires de terres rares, MRu₂Si₂ et MPt₂Si₂. *Comptes Rendus des Seances de l'Academie des Sciences, Serie B: Sciences Physiques*, (286):109–112, 1978.
- [7] A. Bauer, A. Neubauer, W. Münzer, A. Regnat, G. Benka, M. Meven, B. Pedersen, and C. Pfleiderer. Ultra-high vacuum compatible induction-heated rod casting furnace. *submitted*, 2016.
- [8] E. Bauer, N. Pillmayr, E. Gratz, G. Hilscher, D. Gignoux, and D. Schmitt. On the behaviour of the new Kondo lattice CeCuAl₃. *Zeitschrift für Physik B Condensed Matter*, 67:205–210, 1987.
- [9] G. Cordier, E. Czech, H. Schützler, and P. Woll. Structural characterization of new ternary compounds of uranium and cerium. *Journal of the Less Common Metals*, 110(1):327 – 330, 1985.
- [10] A. Das, R.K. Kremer, R. Pöttgen, and B. Ouladdiaf. Magnetic ordering in CeCoGe₃. *Physica B: Condensed Matter*, 378-380:837 – 838, 2006.
- [11] P. K. Das, N. Kumar, R. Kulkarni, S. K. Dhar, and A. Thamizhavel. Anisotropic magnetic properties and superzone gap formation in CeGe single crystal. *Journal of Physics Condensed Matter*, 24(14):146003, April 2012.
- [12] F.R. de Boer, J.C.P. Klaasse, P.A. Veenhuizen, A. Bhm, C.D. Bredl, U. Gottwick, H.M. Mayer, L. Pawlak, U. Rauchschwalbe, H. Spille, and F. Steglich. CeCu₂Ge₂: Magnetic order in a Kondo lattice. *Journal of Magnetism and Magnetic Materials*, 63:91 – 94, 1987.
- [13] M.A. Edwards, S. Horn, and R.D. Parks. Effects of crystal fields on the scaling behavior of the magnetic susceptibility in Ce(Ni_xCu_{1-x})₂Si₂. *Solid State Communications*, 61(1):65 – 69, 1987.
- [14] Louis J. Farrugia. WinGX and ORTEP for Windows: an update. *Journal of Applied Crystallography*, 45(4):849–854, Aug 2012.
- [15] Lars Frik, Dirk Johrendt, and Albrecht Mewis. Eine neue Verzerrungsvariante des CaBe₂Ge₂-Typs—Die Kristallstrukturen von SrPd₂Bi₂, BaPd₂Bi₂ und BaAu₂Sb₂. *Zeitschrift für anorganische und allgemeine Chemie*, 632(8-9):1514–1517, 2006.
- [16] Tobias Görlach. *Tieftemperatureigenschaften der intermetallischen Ce- und Yb-Verbindungen CePtAl₃, La_{1-x}Ce_xCu₆, YbAl₂ und YbPd_{1-x}Pt_xSn*. PhD thesis, Univ. Göttingen, 2006.
- [17] F. Hulliger. On new rare earth gold aluminides LnAuAl. *Journal of Alloys and Compounds*, 200(1-2):75 – 78, 1993.
- [18] Yukihiro Kawamura, Takashi Nishioka, Harukazu Kato, Masahiro Matsumura, Kazuyuki Matsubayashi, and Yoshiya Uwatoko. High pressure electrical resistivity of CeCuAl₃. *Journal of Physics: Conference Series*, 200(1):012082, 2010.
- [19] M. Klicpera and P. Javorský. Study of electronic properties in RCuAu_xAl₃ compounds, where R=Ce, La. *Journal of Magnetism and Magnetic Materials*, 363:88–94, August 2014.
- [20] M. Klicpera, P. Javorský, and M. Diviš. Magnetization and electrical resistivity measurements on CeCuAl₃ single crystal. In *Journal of Physics: Conference Series*, volume 592, page 012014. IOP Publishing, 2015.
- [21] M. Klicpera, P. Javorský, P. Čermák, A. Rudajevová, S. Daniš, T. Brunátová, and I. Čisáková. Crystal structure and its stability in CeCuAl₃ single crystal. *Intermetallics*, 46:126 – 130, 2014.
- [22] M. Klicpera, P. Javorský, and A. Hoser. Structural and electronic properties of RPd₂Al_{2-x}Ga_x (R = Ce and La) compounds. *Journal of Alloys and Compounds*, 596:167–172, 2014.
- [23] M. Kontani, H. Ido, H. Ando, T. Nishioka, and Y. Yamaguchi. Magnetic, Transport and Thermal Properties of CeCuAl₃ Single Crystal. *Journal of the Physical Society of Japan*, 63(5):1652–1655, 1994.
- [24] M. Loewenhaupt, B. D. Rainford, and F. Steglich. Dynamic Jahn-Teller Effect in a Rare-Earth Compound: CeAl₂. *Phys. Rev. Lett.*, 42:1709–1712, 1979.
- [25] S. A. M. Mentink, N. M. Bos, B. J. van Rossum, G. J. Nieuwenhuys, J. A. Mydosh, and K. H. J. Buschow. Antiferromagnetism and crystalfield effects in CeCuX₃ (X=Al,Ga) compounds. *Journal of Applied Physics*, (10):6625 –6627, may 1993.
- [26] S. Mock, C. Pfleiderer, and H. v. Löhneysen. Low-Temperature Properties of CeTAl₃; (T=Au, Cu, Pt) and CeAuGa₃. *Journal of Low Temperature Physics*, 115:1–14, 1999.
- [27] O. Moze and K.H.J. Buschow. Crystal structure of CeCuAl₃ and its influence on magnetic properties. *Journal of Alloys and Compounds*, 245(12):112 – 115, 1996.
- [28] Takahiro Muranaka and Jun Akimitsu. Thermodynamic properties of ferromagnetic Ce-compound, CeAgAl₃. *Physica C: Superconductivity*, 460-462, Part 1(0):688 – 690, 2007.
- [29] A. Neubauer, J. Boeuf, A. Bauer, B. Russ, H. v. Löhneysen, and C. Pfleiderer. Ultra-high vacuum compatible image furnace. *Review of Scientific Instruments*, 82(1):013902, 2011.
- [30] T. Nishioka, Y. Kawamura, H. Kato, M. Matsumura, K. Kodama, and N.K. Sato. High pressure magnetization measurements of -type. *Journal of Magnetism and Magnetic Materials*, 310(2, Part 1):e12 – e14, 2007.
- [31] Igor Oshchapovsky, Volodymyr Pavlyuk, Grygoriy Dmytriv, and Alexandra Griffin. Lanthanum tetrazinc, LaZn₄. *Acta Crystallographica Section C*, 68(6):i37–i40, Jun 2012.
- [32] S. Paschen, E. Felder, and H.R. Ott. Transport and thermodynamic properties of CeAuAl₃. *Eur. Phys. J. B*, 2(2):169–176, 1998.
- [33] Marianne Rotter, Marcus Tegel, Dirk Johrendt, Inga Schellenberg, Wilfried Hermes, and Rainer Pöttgen. Spin-density-wave anomaly at 140 K in the ternary iron arsenide BaFe₂As₂. *Physical Review B*, 78(2):020503, 2008.
- [34] C. Schank, F. Jährling, L. Luo, A. Grauel, C. Wasilew, R. Borth, G. Olesch, C.D. Bredl, C. Geibel, and F. Steglich. 4f-conduction electron hybridization in ternary CeTAl compounds. *Journal of Alloys and*

- Compounds*, 207208(0):329 – 332, 1994.
- [35] Stefan Seidel, Rolf-Dieter Hoffmann, and Rainer Pöttgen. SrPdGa₃ - An orthorhombic superstructure of the ThCr₂Si₂ type. 229(6):6, 2014.
 - [36] Bengt Stebler. The Resistivity Anomaly in Chromium Near the Nel Temperature. *Physica Scripta*, 2(1-2):53, 1970.
 - [37] H Sugawara, S.R Saha, T.D Matsuda, Y Aoki, H Sato, J.L Gavilano, and H.R Ott. Magnetic and transport properties in CeAuAl₃ single crystal. *Physica B: Condensed Matter*, 259-261(0):16 – 17, 1999.
 - [38] Peter Thalmeier and Peter Fulde. Bound State between a Crystal-Field Excitation and a Phonon in CeAl₂. *Phys. Rev. Lett.*, 49:1588–1591, 1982.
 - [39] P. Vonlanthen, J.L. Gavilano, B. Ambrosini, and H.R. Ott. ²⁷Al nuclear magnetic resonance studies of CeAuAl₃. *Physica B: Condensed Matter*, 259-261(0):18 – 19, 1999.
 - [40] Wang Xian-Zhong, Lloret B., Wee Lam Ng, Chevalier B., Etourneau J., and Hangemuller P. Aspects cristallographiques et existence des siliciures ternaires MTSi₃ de structure type BaNiSn₃ (M=Th, Y, Ln et T=Ru, Os, Co, Rh, Ir). 22(6), 1985. Francais.
 - [41] O. S. Zarechnyuk, P.I. Kripyakevich, and E.I. Gladyshevskij. Ternary Intermetallic Compounds with a BaAl₄ Type Superlattice. *Sov. Phys. Crystallogr.*, 9, 1965. translated from Kristallografiya, 9, 835-838 (1964).

	CeAgAl ₃	CeAuAl ₃	CeCuAl ₃	CePdAl ₃	CePtAl ₃
Diffractometer	Stoe IPDS-II	Rigaku Saturn724+	Stoe IPDS-II	Stoe IPDS-II	Rigaku Saturn724+
Radiation	MoK α	MoK α	MoK α	MoK α	MoK α
Wavelength (Å)	0.71073	0.71073	0.71073	0.71073	0.71073
Abs. correction type	empirical	empirical	empirical	empirical	empirical
Abs. coeff. μ	15.737	237.31	16.792	161.11	232.91
Crystal system	orthorhombic	tetragonal	tetragonal	tetragonal	tetragonal
space group	Cmcm	I4mm	I4mm	I4mm	I4mm
a (Å)	6.2050(12)	4.3364(4)	4.2508(4)	12.988(1)	4.3239(4)
b (Å)	10.837(2)	4.3364(4)	4.2508(4)	12.988(1)	4.3239(4)
c (Å)	6.1176(12)	10.8501(15)	10.6436(13)	10.589(1)	10.6670(15)
V (Å ³)	411.38(14)	204.03(4)	192.32 (3)	1786.2(5)	199.43(4)
Z	4	2	2		2
ρ_{calc} (g/cm ³)	5.206	6.805	4.758	5.421	6.930
index range h	-9...9	-5...6	-5...5	-17...17	-6...3
	-16...16	-3...6	-5...5	-17...17	-6...5
	-9...8	-16...14	-14...14	-14...14	-16...16
reflections collected	14323	1821	2475	6685	879
independent reflections	417	226	100	703	141
R _{int} (%)	9.52	3.52	10.49	2.00	3.45
RF2 (%)	6.61	5.25	2.18	8.21	7.60
RF2w (%)	5.45	9.36	5.79	6.29	8.50
RF (%)	3.30	3.78	2.00	5.84	4.81
χ^2	0.369	1.98	1.373	5.84	2.24
no. of free parameters	19	14	14	26	14

Table 3: Experimental details and results of the structure refinement of CeTAl₃ ($T = \text{Ag, Au, Cu, Pd, Pt}$) as studied at ambient conditions.

Atom	Wyckoff	x/a	y/b	z/c	sof	u _{eq}	u ₁₁	u ₂₂	u ₃₃	u ₁₂	u ₁₃	u ₂₃
CeAgAl ₃ , space group <i>Cmcm</i> , a = 6.2050(12) Å, b = 10.837(2) Å, c = 6.1176(12) Å												
Ce	4c	0	0.24552(6)	1/4	1.0	0.0105(4)	0.0097(3)	0.0102(3)	0.0117(5)	0	0	0
Ag1	4c	1/2	0.38336(9)	1/4	0.918(8)	0.0133(5)	0.0125(4)	0.0123(5)	0.0150(6)	0	0	0
Al1	4c	1/2	0.38336(9)	1/4	0.082(8)	0.0133(5)	0.0125(4)	0.0123(5)	0.0150(6)	0	0	0
Al2	4c	1/2	0.1512(4)	1/4	1.0	0.0132(17)	0.0132(17)	0.0154(16)	0.0111(19)	0	0	0
Al3	8e	0.2309(4)	1/2	0	0.96(1)	0.0140(12)	0.0141(10)	0.0132(10)	0.0148(16)	0	0	0.0002(10)
CeAuAl ₃ , space group <i>I4mm</i> , a = 4.3364(4) Å, c = 10.8501(15) Å												
Ce1	2a	0	0	0	1.0	0.0078(7)	0.0068(6)	0.0068(6)	0.0099(7)	0	0	0
Au1	2a	0	0	0.63564(17)	1.0	0.0124(6)	0.0137(6)	0.0137(6)	0.0099(5)	0	0	0
Al1	2a	0	0	0.4064(12)	1.0	0.008(3)	0.003(2)	0.003(2)	0.017(4)	0	0	0
Al2	4b	0	1/2	0.2608(7)	1.0	0.009(3)	0.005(3)	0.011(3)	0.012(3)	0	0	0
CeCuAl ₃ , space group <i>I4mm</i> , a = 4.2508(4) Å, c = 10.6436(13) Å												
Ce1	2a	0	0	0	1.0	0.0063(4)	0.0058(4)	0.0058(4)	0.0071(5)	0.000	0.000	0.000
Cu1	2a	0	0	0.6314(3)	0.84(4)	0.0084(12)	0.0086(13)	0.0086(13)	0.0080(19)	0.000	0.000	0.000
Al1	2a	0	0	0.6314(3)	0.16(4)	0.0084(12)	0.0086(13)	0.0086(13)	0.0080(19)	0.000	0.000	0.000
Al2	2a	0	0	0.4040(8)	1.0	0.0092(15)	0.0062(17)	0.0062(17)	0.015(3)	0.000	0.000	0.000
Al3	4b	0	1/2	0.2489(6)	0.94(4)	0.0081(13)	0.008(3)	0.009(3)	0.0079(14)	0.000	0.000	0.000
CePtAl ₃ , space group <i>I4mm</i> , a = 4.3239(4) Å, c = 10.6670(15) Å												
Ce1	2a	0	0	0	1.0	0.0086(14)	0.0084(12)	0.0084(12)	0.0090(19)	0.00000	0.00000	0.00000
Pt1	2a	0	0	0.6364(3)	0.816(10)	0.0107(11)	0.0127(10)	0.0127(10)	0.0067(13)	0.00000	0.00000	0.00000
Al1	2a	0	0	0.6364(3)	0.184(10)	0.0107(11)	0.0127(10)	0.0127(10)	0.0067(13)	0.00000	0.00000	0.00000
Pt2	2a	0	0	0.3858(12)	0.816(10)	0.034(5)	0.021(3)	0.021(3)	0.060(8)	0.00000	0.00000	0.00000
Al2	2a	0	0	0.3858(12)	0.184(10)	0.034(5)	0.021(3)	0.021(3)	0.060(8)	0.00000	0.00000	0.00000
Al3	4b	0	1/2	0.2566(11)	1.0	0.011(5)	0.010(5)	0.013(5)	0.011(4)	0.00000	0.00000	0.00000

Table 4: Refined fractional atomic coordinates, site occupations as well as equivalent and anisotropic thermal displacement parameters for CeAgAl₃, CeAuAl₃, CeCuAl₃ and CePtAl₃.

Atom	Wyckoff	x/a	y/b	z/c	sof	u _{eq}
(3a) CePdAl ₃ , space group $I4mm$, a = 12.988(1) Å, c = 10.589(1) Å						
Ce1	2a	0	0	0	1.0	0.01266(30)
Ce2	8d	0.3333(4)	0	0.0189(9)	1.0	0.0094(15)
Ce3	8c	0.3291(4)	0.32918	0.012(2)	1.0	0.0129(10)
Pd1	2a	0	0	0.649(2)	1.0	0.0086(17)
Pd2	8d	0.5	0.1653(5)	0.875(2)	1.0	0.0139(25)
Pd3	8c	0.1696(5)	0.16963	0.155(2)	0.65(2)	0.0103(19)
Al1	8c	0.1696(5)	0.16963	0.155(2)	0.34(2)	0.0103(19)
Al2	2a	0	0	0.422(3)	0.78(7)	0.0113
Pd4	2a	0	0	0.422(3)	0.21(7)	0.0113
Al3	4b	0.5	0	0.262(6)	1.0	0.0076(88)
Al4	8d	0.5	0.1687(9)	0.102(2)	0.80(3)	0.0190(57)
Pd5	8d	0.5	0.1687(9)	0.102(2)	0.19(3)	0.0190(57)
Al5	8d	0.5	0.339(3)	0.257(5)	1.0	0.0089(76)
Al6	8d	0.159(3)	0	0.271(5)	1.0	0.0152(89)
Al7	8c	0.154(2)	0.15476	0.882(4)	1.0	0.0241(63)
Al8	16e	0.347(2)	0.168(2)	0.260(3)	1.0	0.0076(51)
(BaNiSn ₃) CePdAl ₃ *, space group $I4mm$, a = 4.34396(6) Å, c = 10.5915(2) Å						
Ce1	2a	0	0	0	1.0	0.0316(8)
Pd1	2a	0	0	0.6247(4)	1.0	0.0410(14)
Al1	2a	0	0	0.3488(12)	1.0	0.0114(11)
Al2	4b	0	1/2	0.2579(8)	1.0	0.0114(11)

Table 5: Refined fractional atomic coordinates, site occupations as well as isotropic thermal displacement parameters for two modifications of CePdAl₃. *results were obtained by the evaluation of X-ray powder diffraction data